The Feel of Virtual Mechanisms

D. Constantinescu

Department of Mechanical Engineering, University of Victoria, Victoria, Canada, danielac@me.uvic.ca

1 Introduction

Typical haptic simulators enable users to feel virtual environments either directly (point interaction [16, 17] or via rigid virtual tools unconnected to other virtual objects (rigid body interaction [5, 9, 12, 13]). However, various applications may require users to manipulate virtual chains. For example, virtual reality-based training for collaborative human-robot manipulations for space missions would re-quire users to feel the forces acting on the payload held by the robot. Virtual prototyping applications may benefit if engineers felt the varying inertia of a mechanism they designed during its intended operation. Haptically-enabled computer games would offer richer interactions if they permitted users to operate virtual chains in addition to single objects. The haptic manipulation of virtual mechanisms calls for the haptic display of mechanism inertia and its joint constraints in addition to its contacts with other objects in the virtual environment.

Currently, little haptics work addresses techniques for enabling users to feel and operate virtual mechanisms. Initial efforts have two primary foci: (i) to develop mechanism simulations with computational performance suitable for single-rate [14] or multi-rate haptic applications [5, 7, 16]; and (ii) to increase the physical accuracy of virtual contact via modeling collisions [2, 17]. The haptic rendering of the complete dynamics of virtual mechanisms is a more recent concern. For admittance-type haptic devices, a method for displaying inertia and joint constraints in addition to contacts is presented in [4]. For impedance-type devices, haptic rendering of joint constraints for serial-chain mechanisms is implemented via proxies with

D. Talabă and A. Amditis (eds.), Product Engineering: Tools and Methods Based on Virtual Reality, 231–242.

first order dynamics in [13]. The haptic display of both joint constraints and inertia is proposed by the author for serial chains [3] and for closed chains [1]. In [1, 3], users feel joint constraints via stiffness control in the null space of the dynamically-consistent inverse of the inertia matrix at the operational point, Λ_h^{-1}. They feel the virtual inertia via impedance control in the range space of Λ_h^{-1}.

The present contribution investigates the effect of the user-selected operational point and of the loop closure constraints on the range and the null spaces of Λ_h^{-1}. Loop closure redundancy is included in the analysis. The paper starts with the overview of the haptic interaction system in Section 2. The properties of Λ_h^{-1} for serial and closed virtual chains are investigated in Section 0. Manipulations of both types of virtual mechanisms illustrate users' perception of the virtual inertia and of the virtual joints in Section 4. Concluding remarks end the paper in Section 5.

2 Haptic Interaction System

The haptic interaction system that displays the feel of virtual mechanisms is schematically represented in Fig. 1. This figure illustrates that the virtual dynamics are simulated in coordinate space and are rendered to users in operational space. Therefore, coordinate space and operational space refer to the virtual mechanism in this paper[1].

Fig. 1 also illustrates that the dynamically consistent inverse of the inertia of the virtual mechanism at the user-selected operational point, Λ_h^{-1}, maps the simulated dynamics from coordinate space to the operational space. Hence, this figure hints that Λ_h^{-1} is key to rendering the feel of virtual mechanisms via impedance haptic devices.

The simulation of the virtual mechanism and the haptic rendering of its dynamics via an impedance haptic device are presented in detail in [1, 3]. Their brief overview in the following two sections focuses on introducing the notation used in the discussion of the structure of Λ_h^{-1} in Section 0.

[1] The coordinate and operational spaces of the mechanism of the haptic device are extraneous to the haptic rendering of the manipulation in as much as the device permits the simulated interaction (i.e., the workspace of the device covers the virtual environment).

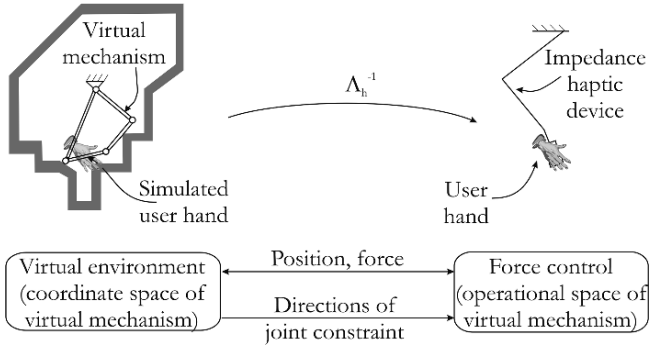

Fig. 1. Haptic interaction system. The dynamics of virtual mechanisms are simulated in coordinate space, and are displayed to users in operational space.

2.1 Mechanism Simulation

In [1, 3], the virtual mechanism manipulated by the user is simulated using extended generalized coordinates [5]. These coordinates are configuration coordinates for serial chains (Fig. 2a). The extended generalized coordinates for closed chains comprise the relative joint coordinates identified after choosing cut joints[2] and cutting them open (Fig. 2b).

In extended generalized coordinates, the dynamics of a mechanism with n links, $m<n$ loop closure constraints and c contacts are:

$$D(q)\ddot{q} + B(q,\dot{q}) + G(q) = \sum_{i=1}^{c} J_i^T(q)F_i + J_h^T(q)F_h - W^T(q)\lambda q \,, \tag{1}$$

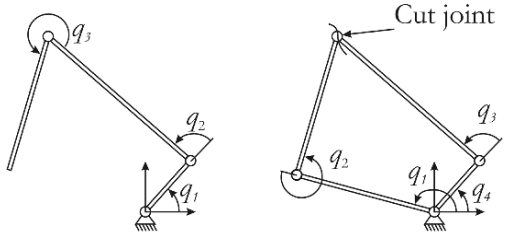

a) Serial chain. **b) Closed chain.**

Fig. 2. Extended generalized coordinates.

[2] Because the selection of cut joints does not affect the feel of the virtual mechanism, it is not addressed in this contribution

where: $D(q)_{n\times n}$ is the inertia matrix of the mechanism in extended generalized coordinates; $B(q,\dot{q})_{n\times 1}$ represent Coriolis and centripetal effects; $G(q)_{n\times 1}$ are gravitational terms; $J_i(q)_{6\times n}$ and $J_h(q)_{6\times n}$ are the mechanism Jacobian computed at the i-th contact and at the user's hand, respectively; $F_{i\ 6\times 1}$ and $F_{h\ 6\times 1}$ are the wrenches applied on the mechanism by the virtual environment at the i-th contact and by the user, respectively; $W(q)_{m\times n} = \partial h/\partial q$ is the rectangular Jacobian of the loop closure constraints; $\lambda_{m\times 1}$ is the vector of Lagrange multipliers, i.e., the vector of constraint forces that maintain the chain closed at the cut joints; and $q_{n\times 1}$, $\dot{q}_{n\times 1}$, $\ddot{q}_{n\times 1}$ are the extended generalized position, velocity, and acceleration of the simulated mechanism, respectively. Eq. (1) represents the dynamics of closed-chain mechanisms if $m > 0$, and the dynamics of serial chains if $m = 0$. These dynamics are augmented with Baumgarte stabilization terms when users manipulate closed-chain mechanisms. Thereafter, the simulation evolves via explicit integration of ODEs regardless whether the mechanism includes closed chains [1] or not [3].

2.2 Control Architecture

During manipulation of virtual mechanisms, users need to feel: (i) the inertia of the mechanism at the selected operational point; (ii) joint constraints when attempting to move along directions restricted by the virtual joints; and (iii) the mechanism contacts with other virtual objects. For manipulations of virtual mechanisms via an impedance haptic device, a control architecture that uses distinct controllers to render the inertia, the joint constraints and the contacts of the virtual mechanism has been introduced in [3]. This architecture, schematically depicted in Fig. 3, comprises three controllers:

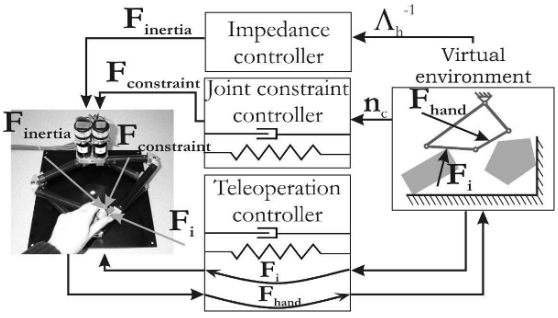

Fig. 3. Schematic of the control architecture that displays the feel of virtual mechanisms via an impedance haptic device.

1. *Impedance controller*: applies to users the inertia of the virtual mechanism at the user-selected operational point. Based on Λ_h^{-1}, this controller shapes the impedance of the haptic device to match the operational space impedance of the virtual mechanism. It renders manipulations unimpeded by the joints or by other objects in the virtual environment.
2. *Joint constraint controller*: resists user's motion along directions n_c restricted by the virtual joints. This stiffness controller uses limited gains to render the infinite structural stiffness of the virtual mechanism along directions in the null space of Λ_h^{-1}.
3. *Four channel teleoperation controller* [11]: enables users to feel contacts through feedforwarding contact forces to users and hand wrenches to the virtual mechanism via the two force channels. It eliminates the drift of the user's hand on the haptic device from the operational point via the two position channels.

The architecture requires Λ_h^{-1} and its null space to adequately render the feel of virtual mechanisms. Singular value decomposition (SVD)-based methods for computing Λ_h^{-1} and its null space are proposed in [3] for serial chains and in [1] for closed chains. In particular:

$$\Lambda_h^{-1} = J_h D^{-1} J_h^T \tag{2}$$

for serial chains, and:

$$\Lambda_h^{-1} = J_h D^{-1} J_h^T - J_h D^{-1} W^T \left(W D^{-1} W^T \right) W D^{-1} J_h^T \tag{3}$$

for closed chains. The significance of these methods for the feel of virtual mechanisms is analyzed in the following section, focusing on the effect of the loop closure constraints and of the user-selected operational point on the structure of the null space of Λ_h^{-1}.

3. Properties of the Dynamically Consistent Inverse of the Operational Space Inertia Of Virtual Mechanisms

The section demonstrates that: (i) Λ_h^{-1} is positive semi-definite both for serial chains and for closed chains; and (ii) redundant loop closure constraints are automatically eliminated when comput-ing the directions of joint constraint using the SVD of Λ_h^{-1} in Eq. (3).

The proof is by construction and uses the positive definiteness of D for any mechanism and for any choice of extended generalized coordinates[3]. Let the SVD of the Jacobian matrix of the loop closure constraints be given by:

$$W_{m\times n} = V_{m\times m} \cdot E_{m\times n} \cdot U^T_{n\times n} = V_{m\times m} \cdot \begin{bmatrix} [\sigma_i]_{r\times r} & 0_{r\times(n-r)} \\ 0_{(m-r)\times r} & 0_{(m-r)\times(n-r)} \end{bmatrix} \cdot U^T_{n\times n} \tag{4}$$

In Eq. (4), $r<m$ is the number of independent loop closure constraints and $[\sigma_i]_{r\times r}$ is a diagonal matrix whose diagonal elements are the r non-zero singular values of. W. Furthermore, the positive definiteness of D implies that a suitable rotation R exists that diagonalizes D^{-1}:

$$D^{-1}_{n\times n} = R^T_{n\times n} \cdot [a_i]_{n\times n} \cdot R_{n\times n}\,, \tag{5}$$

where $[a_i]_{n\times n}$ is diagonal positive definite. After substitution from Eqs. (4) and (5):

$$\begin{aligned} W_{m\times n} \cdot D^{-1}_{n\times n} \cdot W^T_{n\times m} = V_{m\times m} \cdot \begin{bmatrix} [\sigma_i]_{r\times r} & 0_{r\times(n-r)} \\ 0_{(m-r)\times r} & 0_{(m-r)\times(n-r)} \end{bmatrix} \cdot U^T_{n\times n} \cdot \\ \cdot R^T_{n\times n} \cdot [a_i]_{n\times n} \cdot R_{n\times n} \cdot U_{n\times n} \cdot \begin{bmatrix} [\sigma_i]_{r\times r} & 0_{r\times(m-r)} \\ 0_{(n-r)\times r} & 0_{(n-r)\times(m-r)} \end{bmatrix} \cdot V^T_{m\times m} \end{aligned}\,. \tag{6}$$

In Eq. (6), the matrix $Y_{n\times n} = U_{n\times n} \cdot R_{n\times n} = (y_1 \ldots y_n)$ is orthogonal (since $R \cdot U \cdot U^T \cdot R^T = I_{n\times n}$). Therefore, after substitution from Eq. (7):

$$Y^T \cdot A \cdot Y = \begin{pmatrix} y_1^T \\ \vdots \\ y_n^T \end{pmatrix} \cdot [a_i]_{n\times n} \cdot (y_1 \ldots y_n) = [a_{ij} y_i^T \cdot y_j] = A \tag{7}$$

in Eq. (6):

$$\begin{aligned} W_{m\times n} \cdot D^{-1}_{n\times n} \cdot W^T_{n\times m} = V_{m\times m} \cdot \begin{bmatrix} [\sigma_i]_{r\times r} & 0_{r\times(n-r)} \\ 0_{(m-r)\times r} & 0_{(m-r)\times(n-r)} \end{bmatrix} \cdot [a_i]_{n\times n} \cdot \\ \cdot \begin{bmatrix} [\sigma_i]_{r\times r} & 0_{r\times(m-r)} \\ 0_{(n-r)\times r} & 0_{(n-r)\times(m-r)} \end{bmatrix} \cdot V^T_{m\times m} = V_{m\times m} \cdot \begin{bmatrix} [a_i \sigma_i^2]_{r\times r} & 0_{r\times(m-r)} \\ 0_{(m-r)\times r} & 0_{(m-r)\times(m-r)} \end{bmatrix} \cdot V^T_{m\times m} \end{aligned} \tag{8}$$

[3] The positive definiteness of D follows from the fact that kinetic energy $KE = 0.5\dot{q}^T D\dot{q}$ is positive for all $q \neq 0$ for serial and closed chains

and pseudo-inversion of Eq. (8) via SVD:

$$\left(W_{m\times n}\cdot D_{n\times n}^{-1}\cdot W_{n\times m}^{T}\right)^{-1}=V_{m\times m}\cdot\begin{bmatrix}\left[\dfrac{1}{a_i\sigma_i^2}\right]_{r\times r} & 0_{r\times(m-r)}\\ 0_{(m-r)\times r} & 0_{(m-r)\times(m-r)}\end{bmatrix}\cdot V_{m\times m}^{T}. \tag{9}$$

Furthermore:

$$\begin{aligned}
&W_{n\times m}^{T}\cdot\left(W_{m\times n}\cdot D_{n\times n}^{-1}\cdot W_{n\times m}^{T}\right)^{-1}\cdot W_{m\times n}=\\
&=U_{n\times n}\cdot\begin{bmatrix}[\sigma_i]_{r\times r} & 0_{r\times(m-r)}\\ 0_{(n-r)\times r} & 0_{(n-r)\times(m-r)}\end{bmatrix}\cdot\begin{bmatrix}\left[\dfrac{1}{a_i\sigma_i^2}\right]_{r\times r} & 0_{r\times(m-r)}\\ 0_{(m-r)\times r} & 0_{(m-r)\times(m-r)}\end{bmatrix}\cdot\\
&\cdot\begin{bmatrix}[\sigma_i]_{r\times r} & 0_{r\times(n-r)}\\ 0_{(m-r)\times r} & 0_{(m-r)\times(n-r)}\end{bmatrix}\cdot U_{n\times n}^{T}=\\
&=U_{n\times n}\cdot\begin{bmatrix}[\sigma_i]_{r\times r}\cdot\left[\dfrac{1}{a_i\sigma_i^2}\right]_{r\times r}\cdot[\sigma_i]_{r\times r} & 0_{r\times(m-r)}\\ 0_{(n-r)\times r} & 0_{(n-r)\times(m-r)}\end{bmatrix}\cdot U_{n\times n}^{T}=\\
&=U_{n\times n}\cdot\begin{bmatrix}\left[\dfrac{1}{a_i}\right]_{r\times r} & 0_{r\times(n-r)}\\ 0_{(n-r)\times r} & 0_{(n-r)\times(n-r)}\end{bmatrix}\cdot U_{n\times n}^{T},
\end{aligned} \tag{10}$$

and

$$\begin{aligned}
&D_{n\times n}^{-1}\cdot W_{n\times m}^{T}\cdot\left(W_{m\times n}\cdot D_{n\times n}^{-1}\cdot W_{n\times m}^{T}\right)^{-1}\cdot W_{m\times n}\cdot D_{n\times n}^{-1}=\\
&=R_{n\times n}^{T}\cdot[a_i]_{n\times n}\cdot Y_{n\times n}\cdot\begin{bmatrix}\left[\dfrac{1}{a_i}\right]_{r\times r} & 0_{r\times(n-r)}\\ 0_{(n-r)\times r} & 0_{(n-r)\times(n-r)}\end{bmatrix}\cdot Y_{n\times n}^{T}\cdot[a_i]_{n\times n}\cdot R_{n\times n}=\\
&=R_{n\times n}^{T}\cdot[a_i]_{n\times n}\cdot\begin{bmatrix}\left[\dfrac{1}{a_i}\right]_{r\times r} & 0_{r\times(n-r)}\\ 0_{(n-r)\times r} & 0_{(n-r)\times(n-r)}\end{bmatrix}\cdot[a_i]_{n\times n}\cdot R_{n\times n}\\
&=R_{n\times n}^{T}\cdot\begin{bmatrix}[a_i]_{r\times r} & 0_{r\times(n-r)}\\ 0_{(n-r)\times r} & 0_{(n-r)\times(n-r)}\end{bmatrix}\cdot R_{n\times n}.
\end{aligned} \tag{11}$$

Lastly, Λ_h^{-1} of mechanisms with closed chains can be computed after substitution of Eq. (11) in Eq. (3) via:

$$\begin{aligned}\Lambda_h^{-1} &= J_h\left(D^{-1} - D^{-1}W^T\left(WD^{-1}W^T\right)WD^{-1}\right)J_h^T = \\ &= J_h \cdot R^T \cdot \left(\left[a_i\right]_{n\times n} - \begin{bmatrix} \left[a_i\right]_{r\times r} & 0_{r\times(n-r)} \\ 0_{(n-r)\times r} & 0_{(n-r)\times(n-r)} \end{bmatrix} \right) \cdot R \cdot J_h^T = \\ &= J_h \cdot R^T \cdot \begin{pmatrix} 0_{r\times r} & 0_{r\times(n-r)} \\ 0_{(n-r)\times r} & \left[a_{i+r}\right]_{(n-r)\times(n-r)} \end{pmatrix} \cdot R \cdot J_h^T\end{aligned} \tag{12}$$

Eq. (12) reveals the structure of Λ_h^{-1}. This equation shows that Λ_h^{-1} is positive semi-definite for closed chains ($r > 0$), and is positive definite for serial chains ($r = 0$). Furthermore, redundancy in the loop closure constraints ($r < m$) is automatically eliminated via the SVD in Eq. (9).

4 Experiments

The directions of joint constraint computed via SVD of Λ_h^{-1} in Eq (3) are validated via an experiment whereby the user applies a constant wrench $F_h = \begin{pmatrix} -0.5\,\text{N} & 0\,\text{N} & -0.0025\,\text{Nm} \end{pmatrix}^T$ at the operational point of the closed chain shown in Fig. 4. Given the link numbering show in this figure, the parameters of the virtual mechanism are: link lengths $l_1 = l_2 = l_3 = 45$ mm and $l_4 = 60$ mm; link masses $m_1 = m_2 = m_3 = 1\text{kg}$ and $m_4 = .5\text{kg}$; and link inertia $I_1 = I_2 = I_3 = 0.0021$ kgm^2 and $I_4 = 0.00105$ kgm^2.

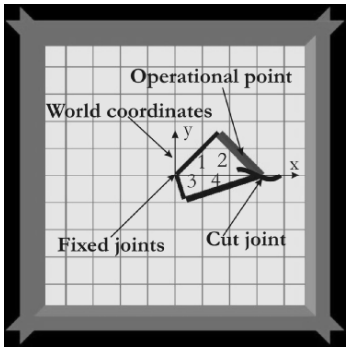

Fig. 4. Testbed used to illustrate the perception of the virtual joints, including those closing kinematic loops.

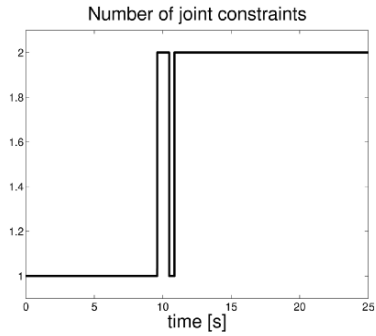

a. Number of virtual joint constraints

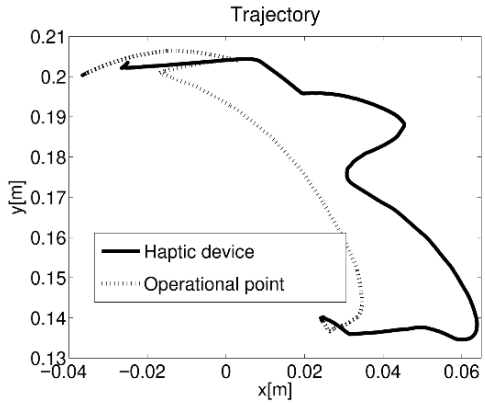

b. Trajectory

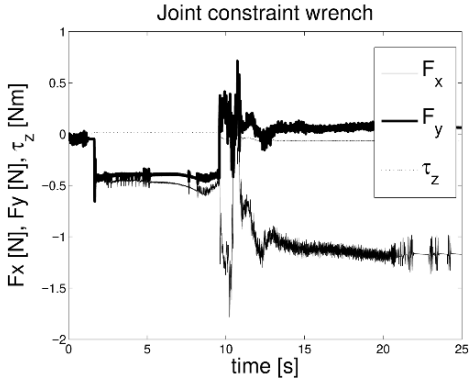

c. Virtual joint constraint to wrench to u

Fig. 5. Experimental results.

The experimental results are plotted in Fig. 5. In particular, Fig. 5a illustrates that users perceive one joint constraint throughout the manipulation. This is because the selected operational point is on a link with insufficient degrees of freedom. When the loop closure constraint becomes active, users perceive two joint constraints. This is expected because the constraint due to the cut joint is independent from the constraint due to the joint between links 1 and 2. Fig. 5b demonstrates that the user hand on the haptic device follows the operational point in the simulation with an error due to the finite stiffness of the joint constraint controller. Lastly, Fig. 5c reveals that users feel a larger constraint wrench when the loop closure constraint is active. This larger perceived wrench is in agreement with the independence of the constraints imposed by the joint between links 1 and 2 and by the cut joint.

The experimental results depicted in Fig. 5 validate that the null space of Λ_h^{-1} provides a basis for the directions of joint constraints regardless whether the joints are cut joints or not.

5 Conclusions

The present contribution elucidates the effect of the loop closure constraints on the null space of Λ_h^{-1}, the dynamically consistent inverse of the inertia matrix of serial-chain and closed-chain mechanisms at an arbitrary user-selected operational point. This effect is important for displaying the feel of virtual mechanisms via impedance-type haptic devices. In particular, haptic rendering methods recently developed by the author enable users to feel the virtual inertia and the virtual joints via separate controllers that operate the in the range space and in the null space of Λ_h^{-1}, respectively. The contribution also demonstrates that redundant loop closure constraints are automatically eliminated by during the SVD Λ_h^{-1}. Users' perception of the virtual joint constraints is illustrated via an experimental manipulation of a closed chain.

Upcoming work will focus on displaying the feel of virtual mechanisms to multiple simultaneous users and on applications to robot control of the dynamically consistent inverse of the inertia matrix.

References

1. Beenakkers M, Constantinescu D, Steinbuch M (2007) Haptic Manipulation of Closed-Chain Virtual Mechanisms. Ac-cepted by IEEE/ASME Int Conf Adv Intell Mechatronics, Zurich, Switzerland.
2. Constantinescu D, Salcudean SE, Croft EA (2005) Haptic Rendering of Rigid Contacts using Impulsive and Penalty Forces. IEEE Trans Robot, 21(3):309-323.
3. Constantinescu D, Salcudean SE, Croft EA (2006) Haptic Manipulation of Serial-Chain Virtual Mechanisms. ASME Trans. J. Dyn. Syst. Meas. Contr., 128(1):65-74.
4. Faulring EL, Lynch KM, Colgate JE, Peshkin MA (2007) Haptic Display of Constrained Dynamic Systmes via Admit-tance Displays. IEEE Trans. Robot., 23(1):101-111.
5. Featherstone R (1987) Robot Dynamics Algorithms.Boston:Kluwer.
6. Gillespie RB (2003) Kane's Equations for Haptic Display of Multibody Systems, Haptics-e, 3(2):1-20.
7. Gillespie RB (2005) On-Line Symbolic Constraint Embedding for Simulation of Hybrid Dynamical Systems, Multibody Dyn. 14: 387-417.
8. Johnson DE, Willemsen P, Cohen E (2005) Six Degree-of-Freedom Haptic Rendering Using Spatialized Normal Cone Search. IEEE Trans Vis Comp Graph, 11(6):661-670.
9. Khatib O (1987) A Unified Approach for Motion and Force Control of Robot Manipulators: The Operational Space Formulation. IEEE Trans Robot Autom, 3(1): 43-53.
10. Kim YJ, Otaduy MA, Lin MC, Manocha D (2003) Six-Degree-of-Freedom Haptic Display Using Localized Contact Computations. Presence: Teleop Virt Env, 12(3):277-295.
11. Lawrence DA (1993) Stability and Transparency in Bilateral Teleoperation. IEEE Trans Robot Autom, 9(5): 624-637.
12. McNeely WA, Puterbaugh KD, Troy JJ (2006) Voxel-Based 6-DOF Haptic Rendering Improvements. Haptics-e, 3(7).
13. Mitra P, Niemeyer G (2004) Dynamic Proxy Objects in Haptic Simulations. In: Proc. IEEE Conf. Robot. Autom. Mechatronics, pp 1054-1059.
14. Nahvi A, Nelson DD, Hollerbach JM, Johnson DE (1998) Haptic Manipulation of Virtual Mechanisms from Mechani-cal CAD Designs. In: Proc. IEEE Int Conf Robot Autom, pp 375-380.
15. Ortega M, Redon S, Coquillart S (2007) A Six Degree-of-Freedom God-Object Method for Haptic Display of Rigid Bodies with Surface Properties. IEEE Trans Vis Comp Graph, 13(3): 458-469.
16. Ruspini DC, Khatib O (1998) Dynamic Models for Haptic Rendering Systems. In: Adv. Robot Kin., pp 523-532.

17. Ruspini DC, Khatib O (1999) Collision/Contact Models for Dynamic Simulation and Haptic Interaction. In: Proc. Int. Symp. Robot. Res., pp 185-195.
18. Zilles CB, Salisbury JK (1994) A Constraint-based God Object Method for Haptic Display. In: Proc. ASME Haptic In-terf Virt Envir Teleop Syst, Chicago, IL, pp 146-150.